Review article

Microphysical properties of atmospheric soot and organic particles: measurements, modeling, and impacts

Check for updates

Weijun Li [1] ✉, Nicole Riemer [2], Liang Xu[3], Yuanyuan Wang[1], Kouji Adachi [4], Zongbo Shi [5], Daizhou Zhang [6], Zhonghua Zheng [7] & Alexander Laskin [8,9] ✉

Atmospheric soot and organic particles from fossil fuel combustion and biomass burning modify Earth's climate through their interactions with solar radiation and through modifications of cloud properties by acting as cloud condensation nuclei and ice nucleating particles. Recent advancements in understanding their individual properties and microscopic composition have led to heightened interest in their microphysical properties. This review article provides an overview of current advanced microscopic measurements and offers insights into future avenues for studying microphysical properties of these particles. To quantify soot morphology and ageing, fractal dimension (D_f) is a commonly employed quantitative metric which allows to characterize morphologies of soot aggregates and their modifications in relation to ageing factors like internal mixing state, core-shell structures, phase, and composition heterogeneity. Models have been developed to incorporate D_f and mixing diversity metrics of aged soot particles, enabling quantitative assessment of their optical absorption and radiative forcing effects. The microphysical properties of soot and organic particles are complex and they are influenced by particle sources, ageing process, and meteorological conditions. Furthermore, soluble organic particles exhibit diverse forms and can engage in liquid–liquid phase separation with sulfate and nitrate components. Primary carbonaceous particles such as tar balls and soot warrant further attention due to their strong light absorbing properties, presence of toxic organic constituents, and small size, which can impact human health. Future research needs include both atmospheric measurements and modeling approaches, focusing on changes in the mixing structures of soot and organic particle ensembles, their effects on climate dynamics and human health.

Airborne aerosol particles undergo physical and chemical transformations over time in the atmosphere, which can significantly alter their properties, including size, morphology, composition, and mixing state[1,2]. External and internal mixtures of soot and organic particles are the most prevalent constituents of tropospheric carbonaceous aerosols. Their origins are intertwined with multi-phase emissions resulting from combustion of fossil fuels and biomass burning[3]. Presently, soot and brown carbon (BrC) in

organic aerosols remain focal research points due to their significant roles and their potential contributions to uncertainty in the atmospheric climate system[4]. A growing body of research is delving into the study of chemistry and microphysics of particles composed of soot and organic mixtures pertaining to diverse atmospheric environments such as remote, urban, ocean, and forested areas, aligned with climate and health impacts in the troposphere[3,5,6]. These studies underscore the necessity for an improved

[1]Key Laboratory of Geoscience Big Data and Deep Resource of Zhejiang Province, Department of Atmospheric Sciences, School of Earth Sciences, Zhejiang University, Hangzhou 310027, China. [2]Department of Climate, Meteorology, and Atmospheric Sciences, University of Illinois at Urbana–Champaign, Urbana, IL, USA. [3]College of Sciences, China Jiliang University, Hangzhou 310018, China. [4]Department of Atmosphere, Ocean, and Earth System Modeling Research, Meteorological Research Institute, Tsukuba, Japan. [5]School of Geography, Earth and Environmental Sciences, University of Birmingham, Birmingham B15 2TT, UK. [6]Faculty of Environmental and Symbiotic Sciences, Prefectural University of Kumamoto, Kumamoto 862-8502, Japan. [7]Department of Earth and Environmental Sciences, The University of Manchester, Manchester, UK. [8]Department of Chemistry, Purdue University, West Lafayette, IN 47907, USA. [9]Department of Earth Atmospheric and Planetary Sciences, Purdue University, West Lafayette, IN 47907, USA. ✉e-mail: liweijun@zju.edu.cn; alaskin@purdue.edu

understanding of their climatic and human health effects, providing motivation for laboratory experiments, test facility studies, and field investigations aimed at advancing fundamental knowledge regarding size, chemical composition, and light absorption properties[7,8]. Despite these efforts, our understanding of the microphysical properties of soot and organic particles remains limited. The microphysical properties and molecular composition of these particles, encompassing size, phase, morphology, and component-specific mixing states, are pivotal in delineating their climatic and health effects[1,9–12].

The aerosol transformation in the atmosphere refers to "ageing process". The description of atmospheric aerosols requires distinguishing two types of their mixing states, the "population mixing state" and the "mixing state of individual particles". Riemer et al.[1] defined population mixing state as the distribution of aerosol chemical species (e.g., SO_4^{2-}, NO_3^-, NH_4^+, various organic components, elemental carbon, and metal elements) among the particles in a given population. This is different from the mixing states of individual particles that one particle contains different aerosol components such as soot, mineral, organic, metal, sulfate, nitrate, etc., and refers to the way that these components are arranged within the particle. Riemer et al.[1] have reviewed the methods of online measurements and the concepts of population mixing state, particularly their relevance to climate-relevant properties. While their review focused primarily on the chemical mixture of atmospheric particles, it did not delve into the potential impacts stemming from the microphysical properties of soot and organic particles. Recent studies reported significant advances in understanding how the microphysical characteristics of soot and organic particles affect their optical absorption and climate-relevant properties[13–15]. However, this knowledge remains fragmented and requires systematic organization. This review manuscript synthesizes the most recent findings and developments in the microphysical properties of soot and organic particles. It also seeks to chart new directions for further investigations of their atmospheric roles, thereby connecting laboratory studies, field research and atmospheric modeling. Additionally, our manuscript presents the first comprehensive summary of the current scientific knowledge in this area. It also provides a roadmap for future investigations into the physical states of these particles and their implications for the atmosphere. This review is mainly concerned with the physical mixing states of individual particles, and we will use the term "mixing structure" for the remainder of the review to avoid confusion with the population mixing state.

Organic components account for a substantial mass fraction of the accumulation mode aerosols, ranging from ~20% to 50% in the continental air[16] and even up to 90% in tropical forest areas[17]. In contrast, black carbon (or soot) particles contribute less than 10% by mass to the fine particles[3]. Soot and organic components of carbonaceous aerosols have become focal points in atmospheric science discussions. Terms such as "black carbon", "soot", "elemental carbon", "equivalent black carbon" and "refractory black carbon" are frequently used interchangeably to describe to the most heat-resistant and light-absorbing component of carbonaceous combustion particles. However, it is important to note that each term has distinct definitions and is associated with different measurement methodologies[18]. In this context, we specifically refer to "soot" from a morphological perspective, characterizing it as agglomerates of carbon spherules composed of graphite-like microcrystallites (Figs. 1 and 2)[19]. While soot inclusions constitute only minor mass fractions of fine atmospheric particles, their cumulative warming effect on the atmosphere through various forcing mechanisms is significant, estimated as +0.11 [−0.20 to 0.42] W m^{-2}[20]. Because of the extensive spatial variability in mass concentrations of soot, ranging from 0.007 to 20 µg m^{-3} on Earth[21–24], their warming effect within polluted areas holds substantial implications for climate change. Moreover, aged soot particles can be coated by secondary aerosol condensation components (e.g., sulfate, nitrate, secondary organics), enhancing optical absorption of aged particles through "lensing effect"[25–27]. In contrast, a majority of organic aerosol components exert overall cooling effect on the Earth's atmosphere with radiative forcing at −0.21 [−0.44 to +0.02] W m^{-2}[20]. However, certain components of the atmospheric organic

mixtures also exhibit significant light absorbing properties, which have been collectively termed as brown carbon (BrC)[6,28,29]. Overall, BrC can contribute up to 50% of mass absorption efficiency[30,31], amplifying the overall radiative forcing effects attributed to carbonaceous aerosol[20]. Therefore, these carbonaceous particles, spanning from nanometers to micrometers in size, significantly influence the climate system and environment by interacting with radiant energy, influencing cloud properties, and impacting human health. The microphysical properties and mixing of soot and organic components of atmospheric particles holds crucial significance for integrating them into atmospheric models and assessing their environmental impact[1,12].

To comprehend the size, phase, morphology, and mixing state characteristics of particles composed of soot and organic components, there is a pressing need for online and offline measurements capable to provide numeric metrics of their external and population internal mixing states as well as an information on the lateral heterogeneity of individual particles[2,10,11,32,33]. Over the past decade, atmospheric models have sought to incorporate particle-specific characteristics of aerosol ensembles for a more comprehensive understanding of their atmospheric implications within the troposphere[1,12]. To improve modeling predictions of particle optical properties, numerous studies have developed a range of numerical optical frameworks, which are discussed in the following section. Additionally, they have compiled extensive metric that encompass various key parameters, such as aggregation structure, refractive index, and particle size dimensions (including both the size of individual microcrystallites and their number in soot particles)[34–38]. Consequently, a review is warranted to consolidate the present scientific advancements and provide insight into the prospective trajectory of understanding the atmospheric state of particles composed of soot and organic components. The following questions necessitate consideration:

What methodologies are viable for observing the phase and mixing structure of carbonaceous particles composed of soot and organic components?

What underlines the primary ageing mechanisms of particle ensembles composed of soot and organic components? How do atmospheric ageing processes alter the mixing structure of the soot-organic particles in polluted air?

How does atmospheric water affect the phase and mixing structure of the soot-organic particle mixtures? To what extent do inorganic constituents impact the phase and mixing characteristics of particles?

How does mixing structures of soot and organics transform the morphology and optical properties of particles, influencing their impact on climate dynamics and human health?

Methodologies for the particle-resolved observations of soot-organic mixtures

Various methodologies have been employed to scrutinize the particle mixing states and phases of characteristics of the soot-organic particle mixtures in the ambient environment. Specifically, real-time characterization of particle shape and mixing state has been demonstrated through concurrent measurements of volume-equivalent and mobility diameter of soot-containing particles using a single-particle soot photometer (SP2, DMT)[39–43]. A centrifugal particle mass analyzer (CPMA) integrated with SP2 (CPMA-SP2) can directly measure the mass of non-refractory coating and soot core based on the coating density and core-shell morphology inferred from the SP2[44,45]. Additionally, custom-built single-particle mass spectrometry, using various laser desorption/ionization methods have been also employed, furnishing size-resolved chemical insights to assess the mixing state of ambient particles composed of soot, organic, and other components[46–49]. Notably, the Soot Particle Aerosol Mass Spectrometer (SP-AMS) has been specially designed and developed to facilitate in-situ measurements of soot particles, but it also provides the chemical compositions of both soot and the non-refractory organic components within the same particles[50]. A number of experimental approaches based on the poke-and-flow technique have been developed to quantify particle viscosity and to
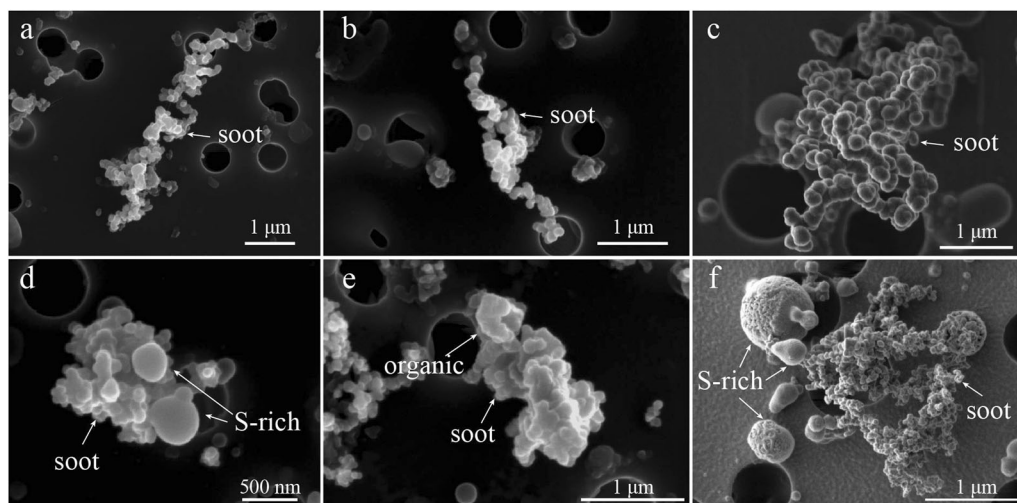
Fig. 1 | The SEM high-resolution images of individual particles containing soot. a, b Two chain-like soot aggregates. **c** Typical aged soot aggregate. **d, f** Mixture of soot and inorganic S-rich components. **e** Mixture of soot and organic components.

investigate the dependence on environmental conditions and particle composition of organic particles[11]. For example, Virtanen et al.[51] developed an electrical low-pressure impactor coupled with a scanning mobility particle sizer and provided the first evidence that aerosol particles smaller than 100 nm could be highly viscous semi-solids or amorphous solids. While these techniques offer real-time particle data and infer the mixing state characteristics of large particle ensembles, they still fall short of providing direct chemical imaging visualization of particle mixing states and heterogeneity of the soot and organic components within individual particles.

Offline electron microscopes have been used in many studies for direct imaging of dry ambient particles collected on the smooth substrates. The scanning electron microscope (SEM) is the instrument of choice for characterizing surface morphology and composition of individual mixed soot-organic particles, albeit with limited capability to delve into inner mixing structures of individual particles[2,10]. Additionally, SEM faces challenges in effectively visualizing fine particles below 100 nm in size (e.g., Fig. 1)[52–55]. The transmission electron microscope (TEM) offers high-resolution imaging, capable of revealing intricate particle details down to atomic scales and directly observing the inner mixing of different chemical components within individual particles (e.g., Figs. 2 and 3a, b). TEM enables efficient observation of the mixing structures of soot, organic and inorganic components within fine particles, as well as the morphological characteristics of individual particles[19,26,56–58].

To further elucidate the mixing structures of inorganic and organic/soot particles, recent studies have harnessed a range of additional microscopic instruments, with applications tailored to their specific research goals. The nanoscale secondary ion mass spectrometry (NanoSIMS) has been employed to examine distribution of organic and inorganic fragment ions on the surface of individual particles above size at 50 nm (Fig. 3c–f)[59,60]. Additionally, scanning transmission X-ray microscope (STXM) coupled with near-edge X-ray absorption fine-structure spectroscopy (NEXAFS) generates chemical images of mixing structures of the soot-organic and inorganic components in individual particles (Fig. 3g–j)[10,61]. These advancements in nanoscale particle analysis significantly enhance our comprehension of how soot-organic components intermingle with atmospheric inorganic salts and dust within individual particles. However, it is important to note that STXM and NanoSIMS have a lower lateral resolution for determining the mixing structure of individual particles compared to the TEM.

Most of the microscopy and chemical imaging methods noted above necessitate the placement of particles within a high-vacuum chamber. It has been recognized that some organic, sulfate and nitrate components may undergo significant transformations induced by drying under high-vacuum

conditions and exposure to the electron beam irradiation (as exemplified by the S-rich component in Fig. 2c), especially in the case of mixed organic and inorganic components[32,58]. To alleviate these limitations, micro-Raman spectroscopy has been employed in some studies to elucidate the mixing structures of carbonaceous and inorganic components in particles, relying on the characteristic vibrational signatures of organic components[62–65]. However, this method encounters constraints because of its much coarser lateral resolution of ~1 μm, which inherently limits chemical component resolution. Emerging as a complementary tool to these high-resolution microscopy techniques, cryogenic transmission electron microscopy (cryo-TEM) has gained prominence. It allows observation of cryo-preserved individual particles composed of organic and inorganic mixtures (as seen in Fig. 3a, b), facilitating more accurate analysis of their mixing structure characteristics[60,66–70]. In essence, the integrated multi-modal microscopic approaches permit the comprehensive characterization of particles' mixing structures, deciphering their soot, organic and inorganic components. In turn, detailed information on particle composition holds potential for advancing our understanding of ageing mechanisms and informing modeling studies.

Microphysical properties of soot particles

Fresh (unaged) soot particles have very distinct morphology and fractal agglomerated structures, which consist of clusters of primary soot nanospheres, typically with approximate diameters of 20 nm. These nanospheres contain distinctive features of concentrically wrapped, graphene-like layers of carbon that aggregate to form larger particles in a grape-like morphology (Figs. 1 and 2)[19,71]. Notably, Fig. 2f illustrates the size distribution of soot particles from various sources, showcasing a typical size range between 40 nm and 2 μm, peaking at ~150–200 nm. Consequently, a significant portion of soot particles have sub-micron sizes, allowing them to remain suspended in the air for extended periods of time. The microphysical property of soot particles comprises two primary aspects: mixing structure and morphology. The fractal dimension (D_f) (illustrated in Fig. 2a–d) serves as a the key parameter for describing the fractal morphology of soot particles[52,72–74]. The D_f of soot particles obtained through the scaling law[72,75] (Eq. (1)), represents a critical morphological attribute, which is mathematically linked to other parameters:

$$N = k_g \left(\frac{2R_g}{R_0}\right)^{D_f} \quad (1)$$

where D_f denotes the fractal dimension, R_g stands for the radius of gyration, k_g represents the fractal factor, R_0 denotes the average radius of the
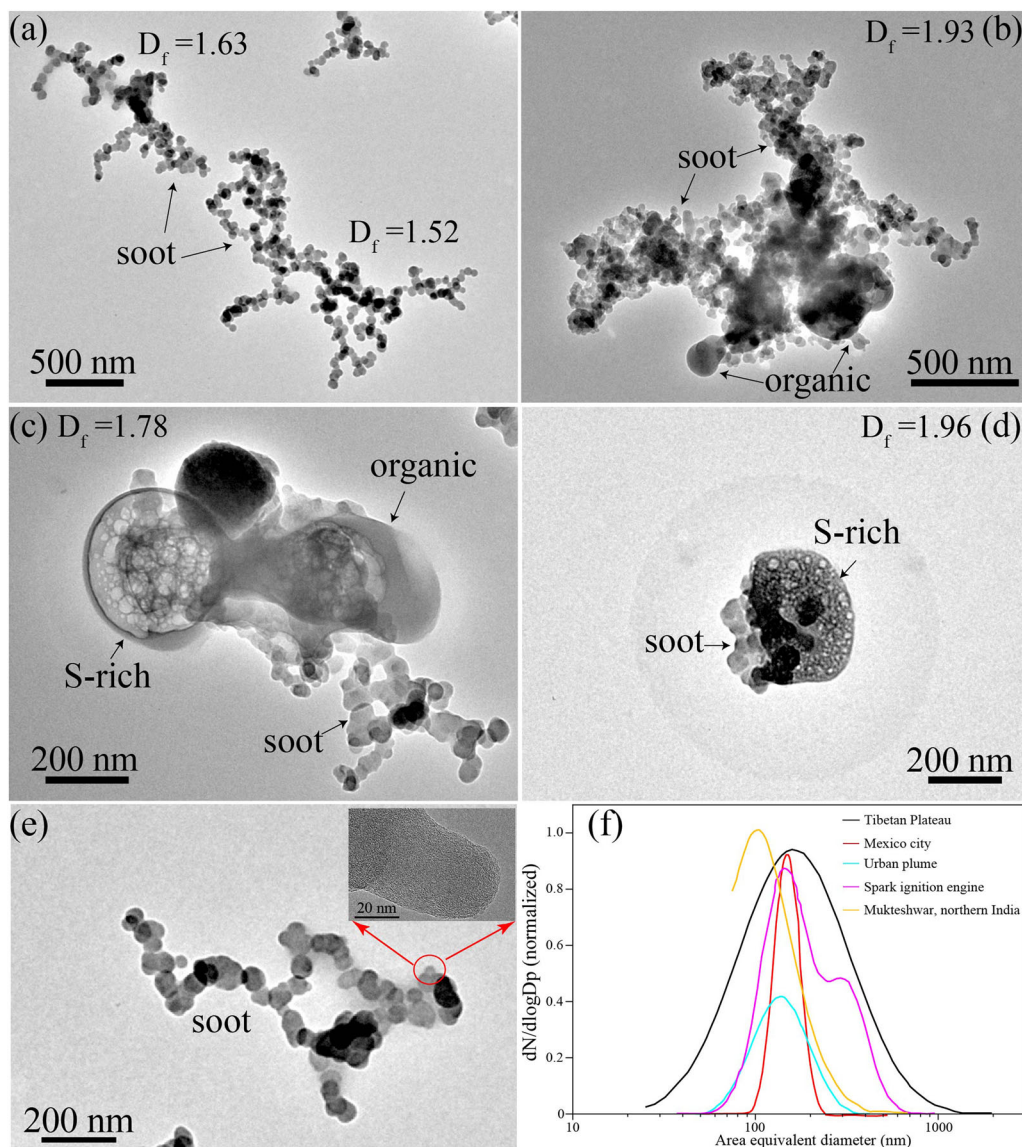
Fig. 2 | The TEM high-resolution images of individual particles containing soot. **a** One chain-like soot aggregate from wood burning. **b** Mixture of soot and organic components from wildfire in rural air. **c** Mixture of soot, organic and secondary components from urban air. **d** Mixture of soot and inorganic components from urban air. **e** Original (unaged) soot particle and the onion microstructure of its monomer, and N is the number of primary nanospheres within the aggregate. A recent report has summarized the details of fractal models and the methodologies for extracting fractal dimensions, a topic that spans various fields of science and mathematics[75]. Here, we will not delve into these methods again, but rather highlight the continued importance of microscopy analysis, particularly for determining D_f, N, and R_0 in internally mixed soot particles through electron microscopy images. Recent advancements in the field have seen the development of innovative computer tools, featuring image recognition techniques and machining learning algorithms to automatically extract microphysical parameters of soot particles from electron microscopy images. This technology progress marks a significant step forward in the study and understanding of soot particles and their characteristics[71,76].

The typical D_f value for aged urban ambient soot particles ranges around 1.82, varying from 1.50 to 2.60[52,56,71,72]. Across different emission sources such as vehicles, biomass burning, and coal combustion, the mean D_f values for unaged soot particles range from 1.66 to 1.77[71]. It is generally individual soot nodule from vehicle emission. **f** Size distribution of soot particles found in the samples from the Tibetan Plateau[176], Mexico City[130], urban plumes[47], a spark ignition engine[72], and in Mukteshwar, northern India[177]. The D_f of individual soot-containing particles was quantified using the method developed by Pang et al.[71].

assumed that the type of combustion source soot particles exerts discernible impacts on soot particles' fractal morphology. Recent studies have underscored the differences in morphological parameters of freshly emitted soot particles originating from different combustion sources, in particular for finer and coarser sizes of soot particles[71,77]. Additionally, many studies reported significant changes in the D_f values related to the atmospheric ageing processes. For example, microanalysis of soot particles has revealed that mixing diversity among soot particles is common in urban and rural air, particularly influenced by emissions from wildfires aged under relative humidity (RH) levels below 80% worldwide[58,74,78,79].

Li et al.[58] introduced the conceptual frameworks outlining the mixing structures of individual soot particles, encompassing "bare-like" (Fig. 2a), "partly coated" (Fig. 2b, c), and "embedded" (Fig. 2d) categories. The D_f for these three categories of soot particles ranged from 1.80 to 2.16 in polluted air, with the order of: "bare-like" < "partly coated" < "embedded"[52,56]. Generally, larger D_f values indicate more compact and aged soot aggregates in the atmosphere. For instance, the D_f value of 1.96 for the compact soot
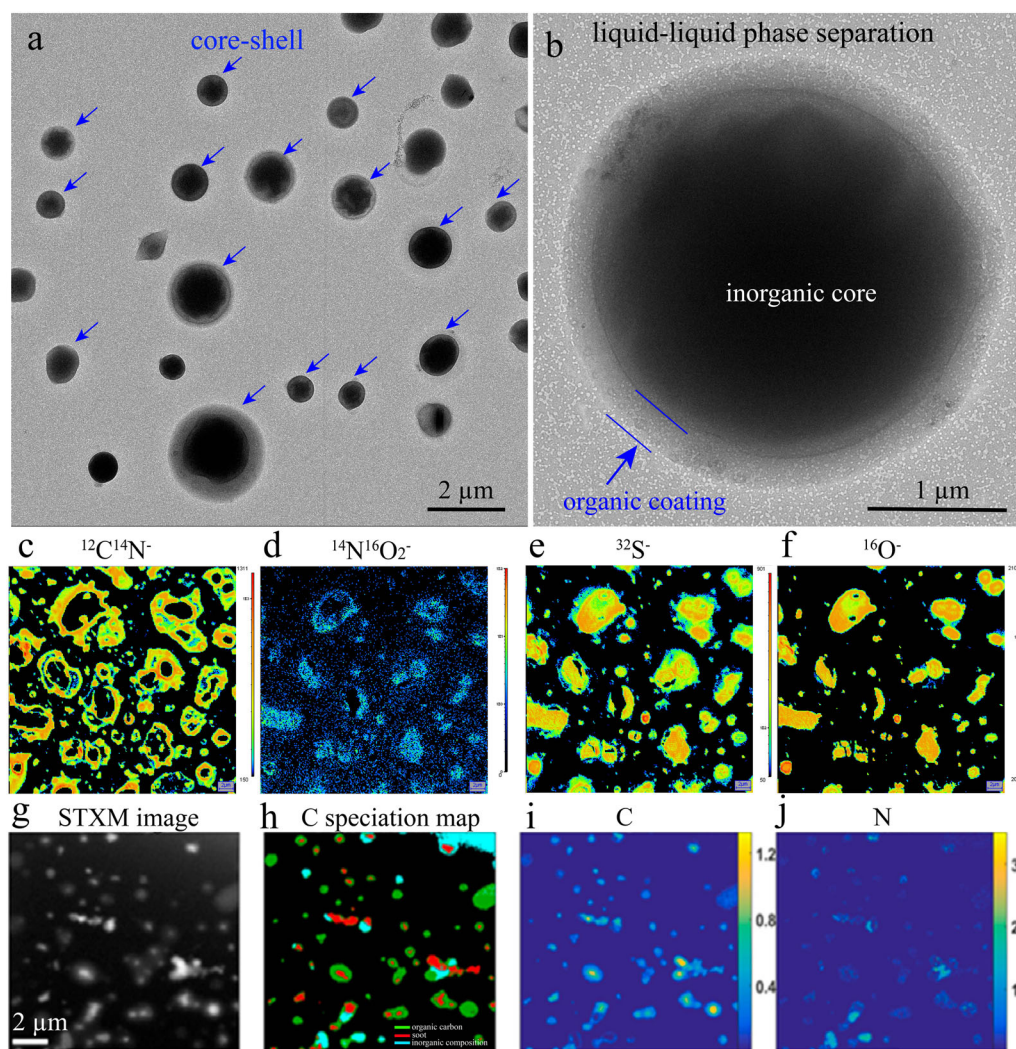
Fig. 3 | Microscopic images showing the liquid–liquid phase separation (LLPS) in mixed organic-inorganic particles. a Cryo-TEM image of the LLPS particles collected at background mountain site. **b** Cryo-TEM image of one typical LLPS particle containing inorganic core and organic coating. **c–f** Ion images of the LLPS particles derived from NanoSIMS showing $^{12}C^{14}N^-$ in the coating, $^{14}N^{16}O_2^-$ in the coating and core, $^{32}S^-$ and $^{16}O^-$ in the core. **g–j** STXM images showing optical images, C speciation map, C, and N elements within individual particles[10,178].

particle (Fig. 2a), is higher than the D_f value of 1.63 for the chain-like soot particle (Fig. 2d), suggesting that soot aggregates tend to collapse during long-range transport[52,71,80]. This collapse and restructuring occur as a result of liquid coatings acquired through condensation during long-range transport[41,81]. Surface tension of water is a prominent factor driving this restructuring during condensation[82–84]. Additionally, some studies proposed that droplet evaporation during atmospheric processes might also contribute to the collapse of the soot aggregates[85,86]. It has been also noted that hygroscopic changes in the coating of soot by secondary aerosol components (i.e., the mixture of organic, nitrate, and sulfate) under varying RH levels is another important factor affecting the D_f values[87]. These coatings can transition from solid to liquid or semi-liquid phases above RH levels of 60–80%[88–91]. In essence, D_f and the coating thickness of soot particles serve as indicators of soot source and ageing in the atmosphere.

Microphysical properties of organic particles

Organic compounds that are emitted directly in particulate form are termed as primary organic aerosols (POAs) (e.g., depicted in Fig. 4). Many volatile organic compounds emitted in the gas-phase undergo atmospheric oxidation yielding semi- or non-volatile ageing products that condense to form secondary organic aerosol (SOA) (as shown in Fig. 5). The microphysical properties of organic particles include two primary aspects, namely their mixing structure and phase state. The latter describes if the particles are liquid, viscous, semi-solids, and amorphous glassy solids. The mixing structure of organic aerosols pertains to how organic matter is internally mixed with inorganic components (as portrayed in Figs. 3 and 4a, b).

Light-absorbing (brown carbon) tarballs[92], a category of the POA particles stemming from biomass burning, coal burning and combustion of heavy fuel oil, adopt a spherical and glassy solids morphology[30,31,93–97]. Tar balls are amorphous and contain no graphitic carbon[98]. Examining Fig. 4 unveils that tarballs display the solid phase and spherical shape of tarballs, as evidenced by SEM images (as illustrated in Fig. 4c, d). The size distribution of tarball particles spans the size range from 80 nm to 2 µm, with the mean values varying between 100 nm, 200 nm, and 300 nm, depending upon their distinct sources (e.g., biomass burning, wood burning, and coal burning) (depicted in Fig. 4f). SEM images captured at substrate tilt of 75° distinguish solid tarballs intermingled with flattened S-rich particles (depicted in Fig. 4c). Upon atmospheric ageing, solid tarballs are relatively inert and serve as primary particles accumulating sulfate, nitrate, and SOA components[58]. Therefore, the ambient tar ball particles are frequently coated by secondary organic components (Figs. 4a, b and 5).

Liquid-like SOA particles within the atmosphere exhibit complex mixing with inorganic components and lack specific morphological characteristics (as depicted in Figs. 2 and 3). These particles demonstrate both
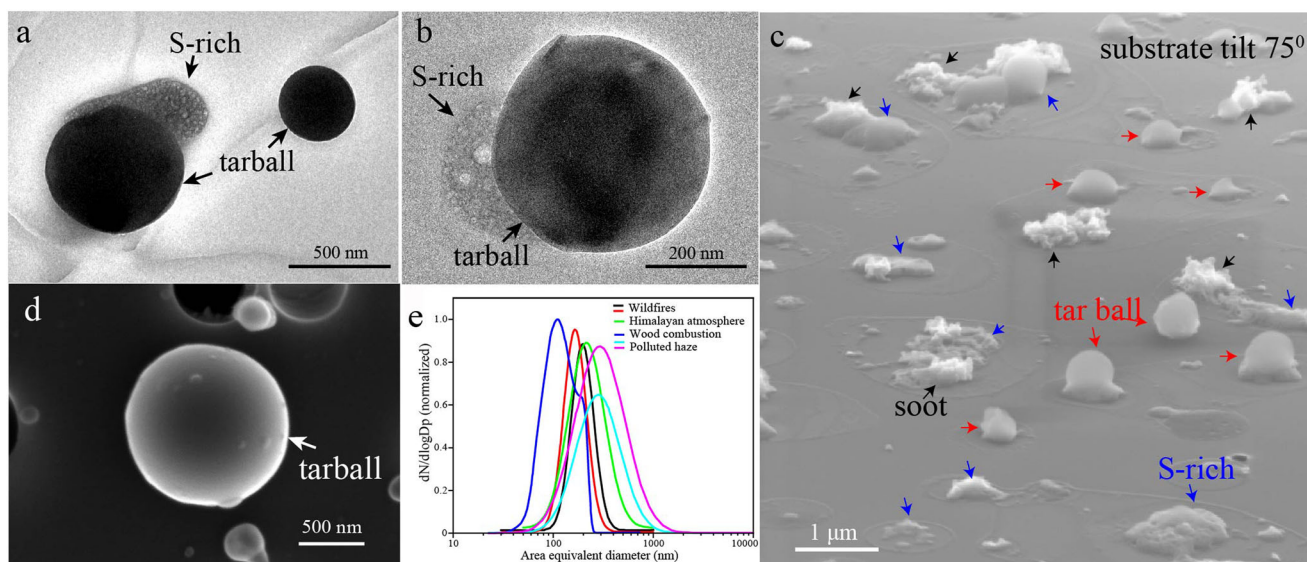
Fig. 4 | High-resolution images of individual tarball particles taken by electron microscopes. a, **b** Mixtures of tar balls coated by inorganic aerosols (S-rich or S-K) (TEM) collected in polluted rural air. **c** SEM image (in the secondary electron mode) of haze samples at 75° tilt angle collected in rural air. Different types of individual particles were marked by the red, green and blue arrows. **d** Externally mixed tarball (SEM) collected in suburban air. **e** Size distributions of tar ball particles collected in wildfires[52]. the Himalayan atmosphere[105], laboratory-generated wood-combustion particles[106], polluted haze air in the Yangtze River Delta and North China Plain of China[81].
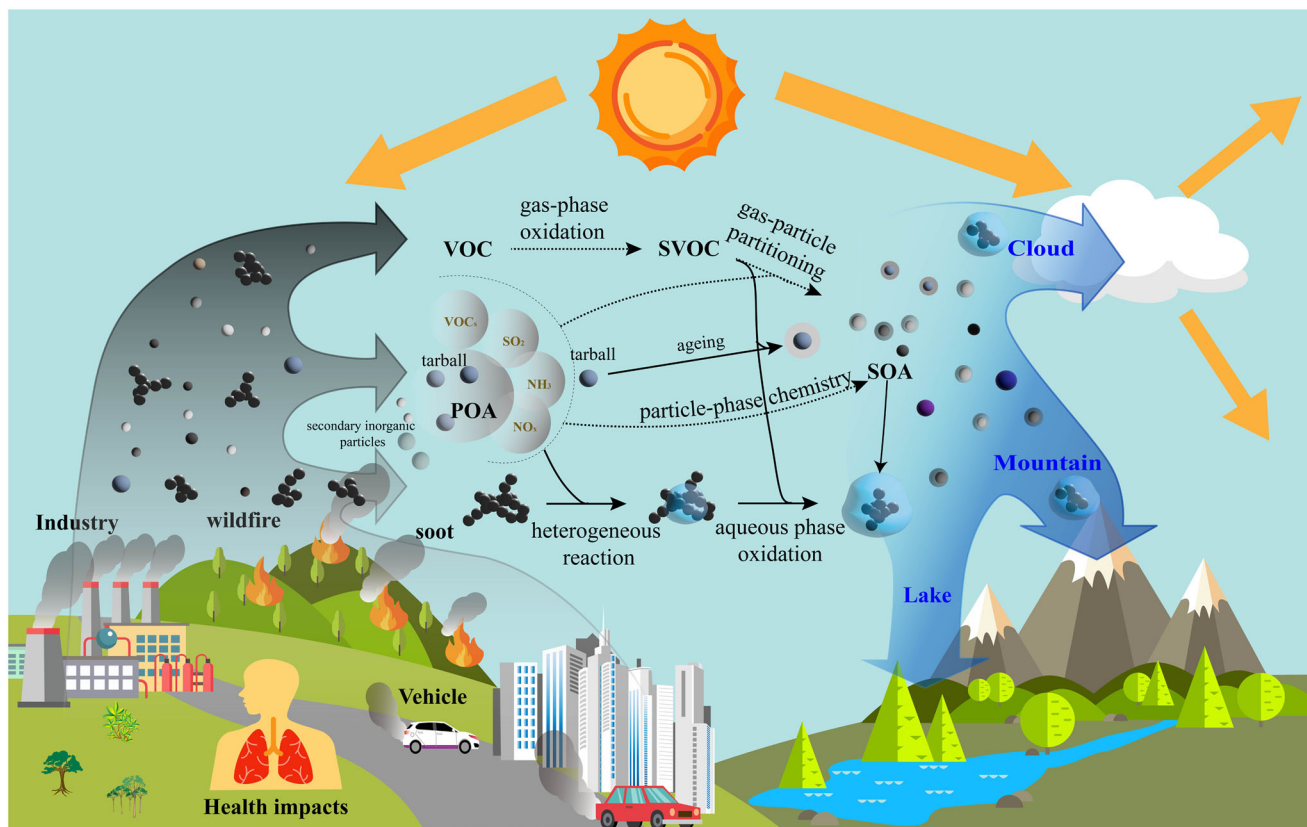

Fig. 5 | Emissions, formations, transports, ageing processes of carboneous aerosol particles in the atmosphere and their impacts on multilayer system of Earth surface. Schematic of emissions and atmospheric ageing process of particles composed of soot and organic components (e.g., tar balls and secondary organic particles) based on morphology and mixing structures in electron images (Figs. 1–4), their sources[16,30,52], transport[81,95,96], chemical formations[19,107], and atmospheric implications[3,25,179].

the SOA-coated and SOA-homogeneous mixing structures[26,58]. The pioneering work of You et al.[99] first introduced the concept of liquid–liquid phase separation (LLPS) between SOA and sulfate components within individual particles, forming core-shell structures. Cryo-TEM and Nano-SIMS images as shown in Fig. 3, both provide evidence of organic matter residing on the particle surface due to the LLPS phenomenon in diverse atmospheric environments, potentially impacting optical, CCN, and heterogeneous reactions on particle surfaces[9,60]. However, these methods are limited in capturing the internal depth of the LLPS mixture (depicted as Fig. 3a–f). An alternative approach employed STXM to assess dimensions of the LLPS in mixed SOA/inorganic particles inferred from the chemically specific spectro-microscopy records acquired along the radial scans of individual particles (depicted in Fig. 3g, h)[61]. The collective integration of these microscopic techniques effectively characterizes LLPS observed for laboratory generated and filter collected ambient particles. To investigate the size-dependent behavior of the LLPS, the cryo-TEM imaging has indicated that the majority of atmospheric particles with diameters exceeding 100 nm display LLPS structure[60,69,70,100]. For example, a field campaign reported an increasing number fraction of LLPS particles as particle size increased beyond 100 nm, with 34% of LLPS particles (by number) in urban air and 55% in rural air in eastern China[60], along with 30% in Arctic air[100]. Various techniques consistently indicate that SOA particles collected at RH conditions of 50%-80% tend to adhere to a substrates upon impact, resulting in their flattening[61,66,96,100]. Consequently, these SOA particles exhibit semi-solid or liquid phase behavior, characterized by their low viscosity values in the ambient air (e.g., as depicted in Fig. 3g, h and indicated by the orange arrow in Fig. 4e). Notably, the direct measurements have highlighted a strong correlation between the SOA phase and relative humidity, as well as particle size[101,102]. Factors influencing the phase and viscosity of SOA and POA (including tar balls) have been comprehensively summarized by Reid et al.[11] and are not expanded upon here.

Atmospheric effects of particles composed of soot and organic mixtures

Light absorption by carbonaceous aerosols. Two primary categories of light-absorbing carbonaceous particles are recognized as BC associated with soot and BrC associated with the light-absorbing components of POA and SOA. Over the past decade, significant advances have been made in utilizing the fractal dimension D_f to quantitatively assess the morphology and mixing structure of soot particles[52,56,71,73,74,77].

Furthermore, practical parameterization schemes have been developed to incorporate these parameters into atmospheric modeling to better understand how the ageing process of soot impact its optical absorption within the atmosphere[13,38,103,104]. Thus, further development of tools to translate measurement parameters or conceptual frameworks into the numerical modeling predications is imperative. Notably, the D_f values can be employed to generate numerical 3D representation of soot particles, which can then be leveraged to calculate the optical absorption by BC fractions of carbonaceous particles[13,26,38,72].

In recent years, researchers have successfully devised several numerical optical models aimed at assimilating D_f, size, and mixing structure of individual soot particles. These include Mie theory[32,102,105–107] (Pathway-1 in Fig. 6)[25,45,108,109], electron tomography with a transmission electron microscope coupled with discrete dipole approximation (ET-DDA)[26] (Pathway-2 in Fig. 6), the Rayleigh–Debye–Gans (RDG) theory[110,111], the superposition T-matrix method (MSTM)[37], the invariant imbedding T-matrix method (Pathway-3 in Fig. 6), the discrete dipole approximation (DDA)[112], and the Single-Particle-Electron-Microscope-to-BC-simulation (SP-EMBS-DDA)[38,71] (pathway 4 in Fig. 6). Each of these pathways presents distinct advantages and disadvantages. Presently, most studies, especially when embedded in large-scale chemistry transport models, have taken a simplified approach by assuming a spherical core-shell representation of complex soot-organic mixed particles (illustrated in Fig. 2d). Despite the simplification, the atmospheric models and measurement studies have reasonably inferred their optical absorption[25,27,45] (Pathway-1 in Fig. 6). The ET-DDA tool directly captures the complex morphology and mixing structure of individual aged soot particles collected on the TEM substrates and subsequently computes their optical properties (as illustrated in Fig. 2a–d). However, this method necessitates a sophisticated and less common TEM setup[26] (Pathway-2 in Fig. 6). Methods of RDG and MSTM can successfully model the fractal morphology of soot aggregates and estimate the parameterization scheme for the cross sections (e.g., extinction, absorption, and scattering), single-scattering albedo (SSA), and asymmetry parameter (g) of pure and aged soot particles, as a function of particle diameter[34–36]. However, these numerical optical models explicitly assume spherical morphology of aged soot particles (Pathway-3 in Fig. 6)[37,113], which is different from more common non-spherical coating shapes shown in Figs. 1 and 2. The recently developed SP-EMBS-DDA serves as a simulation tool that can directly assimilate morphology and mixing structure of aged soot particles shown in electron images from SEM or TEM, leading to the calculation of optical
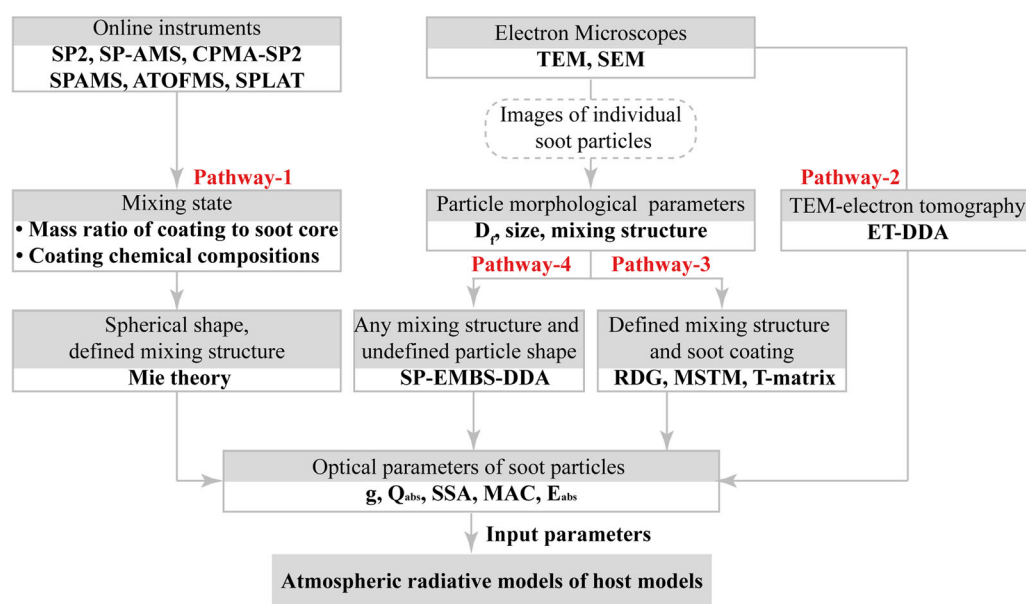

Fig. 6 | The different pathways from ambient measurements to atmospheric radiate models of soot (i.e., black carbon) aerosols. Pathway-1 was acquired from refs. 14, 27, 108, 114, 115, 119, 169,180. Pathway-2 was acquired from ref. 74. Pathway-3 was acquired from refs. 37,110 and Pathway-4 was acquired from refs. 13, 38, 56, 71,77.

properties for soot particles of varying shapes and mixing structures[13]. Notably, the computational efficiency of Pathway-1 using Mie theory is markedly higher compared to other three pathways, which explains its widespread use[38]. The optical models listed above generate optical parameters, such as asymmetry parameter, absorption and scattering coefficients (Q_{abs}, Q_{sca}), and SSA, which are the required inputs for the radiative transfer schemes in atmospheric models (as depicted in Fig. 6).

Aerosol models that are used within chemical transport models differ in their level of detail in which they represent the aerosol, that is they differ in their representation of the population mixing state, as well as in their representation of aerosol thermodynamics and chemistry processes. For example, the Weather Research and Forecasting model with Chemistry (WRF-Chem) is host model for five different aerosol models, a sectional aerosol model (Model for Simulating Aerosol Interactions and Chemistry, MOSAIC, 4 or 8 sections)[114,115], three variations of modal aerosol models (MADE/SORGAM, MADE/VBS, MAM3)[116,117], and a bulk aerosol model (GOCART)[118]. The WRF model has also been coupled with the particle-resolved model PartMC-MOSAIC and to the aerosol two-dimensional bin module for formation and ageing simulation (ATRAS)[1,14,119]. Some of these aerosol modules have also been implemented in global climate models, i.e., MAM3 is used by E3SM, and ATRAS is used by CAM5[120–122]. While the details of the representation of population mixing state differ, they all have in common that they use Mie theory by default to calculate aerosol optical properties, assuming core-shell morphology or volume mixing for BC-containing particles[27]. This implies that the details of morphology and mixing structure are usually not included to the extent that more sophisticated optical models would be able to. Some targeted studies exist that explore the importance of more complicated mixing structures for aerosol optical properties within large-scale models. For example, Adachi et al.[26] used the Goddard Institute for Space Studies General Circulation Model II-prime to show that the core-shell model assumption leads to an overestimation of the radiative forcing on the order of 20% compared to using DDA calculation. On the other hand, assuming uncoated spherical or aggregated soot particles underestimates the radiative forcing by ~30%. In simulations with a regional CTM, Andersson and Kahnert[123] use different optical models depending on the simulated mixing state of black carbon. They treated externally-mixed black carbon as fractal aggregates. For internally-mixed black carbon, they used the "core-grey-shell" model, which uses spherical geometry but parameterizes the coating effect of a black carbon-containing particle by distributing the black carbon mass between the spherical core and the homogeneously mixed shell[124]. They concluded that the more detailed description of particle morphology and mixing state impacted the aerosol optical properties to a similar degree as the inclusion of aerosol-microphysical processes.

Over the past decades, numerical modeling studies have demonstrated that enhancing the accuracy of D_f and mixing structure significantly improves the evaluation of atmospheric optical effects of soot particles[1,3,13,26,111,113,124,125] and even for particles containing BrC[126–128]. Beyond the fractal morphology of soot particles[129], coating thickness, including that of BrC, has been recognized as a critical factor in determining the optical absorption enhancement of internally mixed soot particles due to the lensing effect[25,45,47,104,109,130–132]. While significant progress has been made in understanding the ageing of light absorbing particles, divergent results from ambient optical measurements or the optical modeling of soot continue to emerge[20]. An additional challenge arises from the heterogeneous mixing diversity of soot particles, where different embedded fractions between soot and non-soot components within individual particles can lead to discrepancies of 14–51% in soot absorption enhancement[13,14,39,46,127,133]. Notably, for fully coated soot particles, a hypothesis has been emerged suggesting that LLPS can lead to soot redistribution and weakening the optical absorption of soot-containing particles[69], countering the conventional understanding that increased coating thickness in aged soot results in higher optical absorption enhancement. In the UV region, when considering the coating to consist of strongly absorbing BrC in liquid–liquid phase separation particles (Fig. 3b), there is a notable impact on their optical

properties. Specifically, the scattering cross sections of these particles can be up to 50% larger compared to those of homogenously mixed particles while their absorption cross sections may be reduced by up to 20%[134]. This variance highlights the significant influence of particle composition and structure on their optical behavior in the UV spectrum. The evolving comprehension of ageing in light-absorbing carbonaceous aerosols underscores the present need for validation and refinement of existing models that address the microscale changes in individual particles affecting light scattering and absorption[122,133,135].

Impacts on radiative forcing
The radiative forcing of light-absorbing carbonaceous aerosols has become a central focus within the scientific community, owing to its direct connection with the global warming of climate[8,136,137]. However, accurate prediction of the global radiative forcing of soot particles has remained a contentious issue for decades. Various studies have reported conflicting values for the direct radiative forcing (DRF) of soot-containing particles. For instance, different studies have suggested global mean DRF values of +0.55 W m^{-2} and +0.71 (+0.08 to +1.27) W m^{-2} in different studies[3,27]. Conversely, alternative reports suggested smaller DRF of +0.23 (+0.06 to +0.48) W m^{-2} by Myhre et al.[138], +0.11 (effective radiative forcing; the range of −0.20 to +0.42) W m^{-2} by IPCC[20], and +0.15 ± 0.17 W m^{-2} by Thornhill et al.[139]. When evaluating the direct radiative forcing (DRF) of aged soot particles, taking into account factors such as the core-shell structures and heterogeneity (including variations in shape and the position of the soot core), there is a notable change in the global DRF of soot particles. Specifically, the DRF decreases from 0.30 ± 0.01 to 0.23 ± 0.01 W m^{-2}, corresponding to about a 23% fractional change[133]. Despite concerted efforts to refine DRF estimates, the contribution of soot-containing particles to the uncertainty of climate models remains substantial ~90%[3], thereby constraining predictive accuracy.

Numerous studies have undertaken comprehensive investigations to delve into the actual radiative properties of soot-containing particles, leveraging improved insights into factors such as aerosol concentration[140], lifetime[136,140,141], ageing mechanism[109,140], vertical structure[141,142], and mixing state[111,143,144]. For example, Wang et al.[140] reduced the global mean atmospheric lifetime of soot from 5.1 to 4.4 days and differentiated soot lifetime based on emission sources and pollution levels. The DRF uncertainty linked to soot mixing structure mitigated by incorporating the core-shell model of soot particles into climate models[144]. In a bid to refine the representation of mixing structure, climate models have incorporated the core-shell particles with diverse sizes and more intricate mixing structures (Fig. 7)[15,111,135,143].

As attention shifted toward the absorption capacity of BrC, efforts were made to estimate the direct radiative effect of BrC within global models[29,145–147]. Such estimates of the direct radiative effect have varied, spanning from +0.03 to +0.6 W m^{-2}[29,140,145,147,148]. Nevertheless, the parameterization scheme employed in these models have generally been simplified and unable to fully account for BrC's absorption behavior across wavelength, as well as its variability related to factors such as sources and mixing structure[145,149,150]. Furthermore, the assessment of BrC's radiative forcing in models still grapples with a shortage of input data because of the lack of spectrally resolved light scattering and absorption data for BrC relevant to various emission sources. Therefore, the estimates of BrC's impact within the global models remain burdened by considerable uncertainty.

Impacts on clouds
Model estimates suggest that aerosols resulting from human activities caused an increase in the scattering and absorption of solar radiation by a range of 14–29% as well as an increase of cloud droplet number concentration by a range 5–17% during the period of 2005–2015 in comparison to the year 1850[151]. Soot-containing particles, as potent absorbing aerosols, have a considerable influence on radiative forcing through both direct and indirect effects[20]. Certain particles containing soot can even serve as ice nucleating particles (INP) within cirrus clouds and mixed-phase
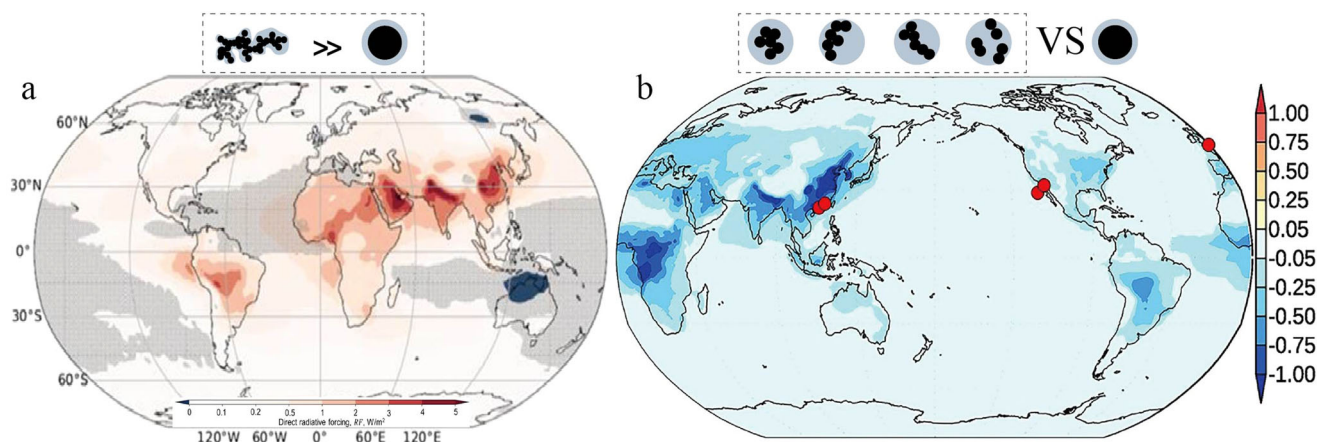
Fig. 7 | Global maps of the direct radiative forcing of climate models. a The assumptions of coated spheres versus realistic agglomerates estimated by ECHAM-HAM. Accounting for the realistic morphology of coated soot increases its direct radiative forcing affect by 22% on average. **b** Simulated global mean soot DRF near the surface from four mixture structures of soot absorption estimated by NCAR CESM1. The global mean soot DRF change is ~0.07 W m^{-2}, corresponding to ~23% reduction. The figures are adapted with permission from Kelesidis et al.[111] and Huang et al.[135].

clouds[152,153]. Freshly emitted soot particles have ice-nucleating ability at −30 °C and exhibits significant variability from various sources yielding greater INP concentration[154]. Initially, freshly emitted soot particles exhibit hydrophobic characteristics, while atmospheric ageing processes involving condensation of trace gases and oxidation can lead to increased hygroscopicity of aged soot[84,155]. These mixing attributes of soot particles are closely tied to their interactions in aerosol-cloud processes[156,157]. In cloud droplet residuals, soot particles have been detected, indicating their impact on cloud activation and contribution to CCN[103,158,159]. On average, the cloud radiative response to soot particles encompasses both indirect and semi-direct effects. Koch et al.[160] indicate a positive cloud response because soot particles provide a deposition sink for secondary aerosols, thereby reducing the nucleation and evolution of viable CCN. Theoretical calculation have recently illustrated that alternations in soot mixing structures and morphological characteristics due to the cloud process can result in an increase of light absorption by a factor of 1.57 to 2.01[103]. Furthermore, Lohmann et al.[136] presented global climate simulations revealing that soot ageing led to the augmentation of thick, low-level clouds, which in turn decreased negative shortwave effective radiative forcing by 0.2 to 0.3 W m^{-2}, compared to pre-industrial conditions. Therefore, the interplay between soot and clouds in the troposphere (as shown in Fig. 5) remains a complex and open question due to wide variability of emission sources and ageing mechanisms affecting soot particles.

Organic matter is widely observed within atmospheric cloud droplets. The organic coatings illustrated in Fig. 4 include both hydrophilic and hydrophobic constituents, including organic acids and diacids, proteins, and humic-like substances[161]. The presence of an organic coating at the gas–liquid interface of aerosols can potentially impact the aerosol's ability to act as CCN by depressing surface tension[162,163]. Additionally, presence of organic layers can enhance ice nucleation within the droplets by providing a template for hexagonal ice[164]. Notably, there is evidence suggesting that organic aerosol particles can act as CCN without the need for inorganic material mixing[159]. In a context of droplet activation, the hygroscopic properties of organics are governed less by solubility and more by the molecular weight of the organic species[162,163]. Consequently, it becomes important to grasp the organic mixing structures and molecular weights as they relate to the ageing process of atmospheric aerosols[107].

Other possible effects
Light-absorbing aerosol particles (as shorter-lifetime aerosols) undergo removal through both dry and wet depositions and change the reflectivity of snowpacks and glacier surfaces, as illustrated in Fig. 5. A recent focal point of investigation involves gaining a comprehensive understanding of the

intricate relationship between deposits of the light-absorbing aerosols (e.g., soot, BrC, and mineral dust) in the snow albedo reduction. Snow strongly reflects sunlight, while the reflection extent depends strongly on factors such as the snow grain size and morphology and the mixing state of soot with the snow matrix. Although few reports considered mixing structures of soot particles in the glacier–snowpack atmosphere[165], no study investigated their actual mixing structures in snowpacks. Specifically, a model study from He et al.[166] assumed internal mixing of soot particles within snow and found a substantial reduction in snow albedo, with the factors of 1.2 to 2.0, depending on the content of soot content and the shape of snow gains.

Soot and organic particles, as depicted in Fig. 5, play a pivotal role in exacerbating air quality issues and contribute substantially to the worldwide public health challenges. Soot particles, dominating within the size range of 50–500 nm (Fig. 2f), comprise large fractions of polycyclic aromatic hydrocarbons (PAHs) and various other toxic hydrocarbons[167]. The mixing state of soot and organic particles has the potential to exacerbate the associations between associations between soot/organic exposure and health effects, as it influences particle properties such as water solubility, surface characteristics, and size-related deposition efficacy within the respiratory tract[168].

While this review does not cover the broad topic of the impact of soot and organic particles on snow/ice and human health, it is important to mention a notable gap in the field. Currently, there is a scarcity of data describing the microphysical properties of soot and organic particles, with limited information inferred from various empirical and theoretical considerations. This lack of real-world data highlights a critical area for future research and underscores the need for more in-depth studies in this domain.

Summary and future perspectives
The physical and chemical characteristics of soot and organic particles undergo significant alternations as a result of atmospheric ageing. In this review, we delved into their physical attributes, including morphology, mixing structure, and phase, within diverse atmospheric conditions and discussed their implications influences on climate, CCN formation, and human health. The considerable attention directed toward light-absorbing carbonaceous particles in the climate system stems from their strong light-absorption properties.

However, the accurate estimation of optical absorption remains a challenge, with significant uncertainties across all scales—local, regional, and global. These uncertainties can be attributed to several factors: (1) Current atmospheric models struggle to incorporate complex microphysical parameters of particles derived from various field measurements. (2) Discrepancies arise from the diverse array of online and offline measurements that yield different parameter values for explaining the optical

absorption of soot and BrC. (3) Beyond the microphysical property of light-absorbing particles, their chemical composition, particularly BrC undergoes continuous changes due to atmospheric ageing or variations arising from different formation pathways and sources. (4) Improved optical models of realistic mixing structures are required to accurately predict the optical properties of aged soot and organic particles, particularly those exhibiting complex mixing structures and morphologies. The implementation of these advanced techniques can significantly decrease the computation time and facilitate the creation of extensive optical database for climate models[169–173]. As atmospheric models progress and advanced instruments evolve, it is expected these discrepancies in description of soot and BrC characteristics will gradually diminish.

While understanding of the chemical composition of soot and BrC is critical for characterizing their atmospheric, recent years have witnessed increased interest in the microphysical properties of these particles, bolstered by a refined understanding of individual particles properties[1,2,11]. The review underscores the significance of the microphysical properties of individual particles in determining atmospheric optical changes, CCN behavior, and health impacts (Fig. 5). Recent studies have unveiled novel phenomena such as LLPS, intricate mixing structure, soot redistribution, and diverse physical phases (solid, semi-solid, liquid) of organic particles. In line with these insights into individual particles properties, innovative applications of chemical imaging tools like Cryo-TEM, NanoSIMS, STXM-NEXAFS, and Aerosol optical Tweezers have been employed to advance aerosol science[2,9,59–61,174]. Moving forward, future research should prioritize the development of advanced microscopic approaches to better observe the microphysical properties and chemical compositions of large samples of individual particles. An example is atomic force microscopy-based infrared spectroscopy (AFM-IR), an emerging technique that enables chemical analysis and compositional mapping with nanoscale resolution under ambient conditions[175]. Moreover, integrating various microscopic techniques offers an efficient approach to comprehensively understand the microphysical properties of individual particles.

Building upon the improved understanding of experimental measurements for individual particles, novel numerical models have emerged, enabling precise accounting for complex soot particle properties, such as shape and mixing structures. Experimental methods like SP[71], EMBS-DDA[13,38], and ET-DDA[26] have greatly enhanced our grasp of how the microphysical properties of soot and organic particles influence optical absorption, cloud forming propensity and health implications[168]. However, a gap remains in incorporating these physical and chemical attributes of aerosol particles into atmospheric models. Future research should strive to establish a refined framework for comprehending the physical and mixing structure characteristics of soot and organic particles, facilitating improved measurements of microphysical ageing process on a global scale.

References

1. Riemer, N., Ault, A. P., West, M., Craig, R. L. & Curtis, J. H. Aerosol mixing state: measurements, modeling, and impacts. *Rev. Geophys.* **57** https://doi.org/10.1029/2018RG000615 (2019).
2. Li, W. et al. A review of single aerosol particle studies in the atmosphere of East Asia: morphology, mixing state, source, and heterogeneous reactions. *J. Clean. Prod.* **112**, 1330–1349 (2016).
3. Bond, T. C. et al. Bounding the role of black carbon in the climate system: a scientific assessment. *J. Geophys. Res.* **118**, 5380–5552 (2013).
4. Li, J. et al. Scattering and absorbing aerosols in the climate system. *Nat. Rev. Earth Environ*. https://doi.org/10.1038/s43017-022-00296-7 (2022).
5. Coppola, A. I. et al. The black carbon cycle and its role in the Earth system. *Nat. Rev. Earth Environ*. https://doi.org/10.1038/s43017-022-00316-6 (2022).
6. Laskin, A., Laskin, J. & Nizkorodov, S. A. Chemistry of atmospheric brown carbon. *Chem. Rev.* **115**, 4355–4382 (2015).
7. Wang, Q. et al. Review of brown carbon aerosols in China: pollution level, optical properties, and emissions. *J. Geophys. Res.* **127**, e2021JD035473 (2022).
8. Yue, S. et al. Brown carbon from biomass burning imposes strong circum-Arctic warming. *One Earth* **5**, 293–304 (2022).
9. Freedman, M. A. Liquid–liquid phase separation in supermicrometer and submicrometer aerosol particles. *Acc. Chem. Res.* **53**, 1102–1110 (2020).
10. Laskin, A., Moffet, R. C. & Gilles, M. K. Chemical imaging of atmospheric particles. *Acc. Chem. Res.* **52**, 3419–3431 (2019).
11. Reid, J. P. et al. The viscosity of atmospherically relevant organic particles. *Nat. Commun.* **9**, 956 (2018).
12. Shrivastava, M. et al. Recent advances in understanding secondary organic aerosol: implications for global climate forcing. *Rev. Geophys.* **55**, 509–559 (2017).
13. Wang, Y. et al. Nonlinear enhancement of radiative absorption by black carbon in response to particle mixing structure. *Geophys. Res. Lett.* **48**, e2021GL096437 (2021).
14. Fierce, L. et al. Radiative absorption enhancements by black carbon controlled by particle-to-particle heterogeneity in composition. *Proc. Natl Acad. Sci. USA* **117**, 5196–5203 (2020).
15. Wang, J. et al. Unified theoretical framework for black carbon mixing state allows greater accuracy of climate effect estimation. *Nat. Commun.* **14**, 2703 (2023).
16. Kanakidou, M. et al. Organic aerosol and global climate modelling: a review. *Atmos. Chem. Phys.* **5**, 1053–1123 (2005).
17. Chen, Q. et al. Mass spectral characterization of submicron biogenic organic particles in the Amazon Basin. *Geophys. Res. Lett.* **36** https://doi.org/10.1029/2009gl039880 (2009).
18. Petzold, A. et al. Recommendations for reporting "black carbon" measurements. *Atmos. Chem. Phys.* **13**, 8365–8379 (2013).
19. Buseck, P. R., Adachi, K., Gelencsér, A., Tompa, É. & Pósfai, M. Ns-soot: a material-based term for strongly light-absorbing carbonaceous particles. *Aerosp. Sci. Technol.* **48**, 777–788 (2014).
20. IPCC. in *Climate Change 2021: The Physical Science Basis* (eds Masson-Delmotte, V. et al.) 817–922 (Cambridge University Press, 2022).
21. Cao, J.-J. et al. Black carbon relationships with emissions and meteorology in Xi'an, China. *Atmos. Res.* **94**, 194–202 (2009).
22. Metcalf, A. R. et al. Black carbon aerosol over the Los Angeles Basin during CalNex. *J. Geophys. Res.* **117**, D00V13 (2012).
23. Sharma, S. Long-term trends of the black carbon concentrations in the Canadian Arctic. *J. Geophys. Res.* **109** https://doi.org/10.1029/2003jd004331 (2004).
24. Dai, M. et al. Long-term variation and source apportionment of black carbon at Mt. Waliguan, China. *J. Geophys. Res.* **126**, e2021JD035273 (2021).
25. Cappa, C. D. et al. Radiative absorption enhancements due to the mixing state of atmospheric black carbon. *Science* **337**, 1078–1081 (2012).
26. Adachi, K., Chung, S. H. & Buseck, P. R. Shapes of soot aerosol particles and implications for their effects on climate. *J. Geophys. Res*. **115** https://doi.org/10.1029/2009JD012868 (2010).
27. Jacobson, M. Z. Strong radiative heating due to the mixing state of black carbon in atmospheric aerosols. *Nature* **409**, 695–697 (2001).
28. Poschl, U. Atmospheric aerosols: composition, transformation, climate and health effects. *Angew. Chem. Int. Ed.* **44**, 7520–7540 (2005).
29. Jo, D. S., Park, R. J., Lee, S., Kim, S. W. & Zhang, X. A global simulation of brown carbon: implications for photochemistry and direct radiative effect. *Atmos. Chem. Phys.* **16**, 3413–3432 (2016).
30. Chakrabarty, R. K. et al. Shortwave absorption by wildfire smoke dominated by dark brown carbon. *Nat. Geosci.* **16**, 683–688 (2023).

31. Corbin, J. C. et al. Infrared-absorbing carbonaceous tar can dominate light absorption by marine-engine exhaust. *npj Clim. Atmos. Sci.* **2** https://doi.org/10.1038/s41612-019-0069-5 (2019).

32. Ault, A. P. & Axson, J. L. Atmospheric aerosol chemistry: spectroscopic and microscopic advances. *Anal. Chem.* **89**, 430–452 (2017).

33. Shao, L. et al. A review of atmospheric individual particle analyses: methodologies and applications in environmental research. *Gondwana Res.* **110**, 347–369 (2022).

34. Liu, C., Xu, X., Yin, Y., Schnaiter, M. & Yung, Y. L. Black carbon aggregates: a database for optical properties. *J. Quant. Spectrosc. Radiat. Transf.* **222–223**, 170–179 (2019).

35. Smith, A. J. A. & Grainger, R. G. Simplifying the calculation of light scattering properties for black carbon fractal aggregates. *Atmos. Chem. Phys.* **14**, 7825–7836 (2014).

36. Romshoo, B. et al. Optical properties of coated black carbon aggregates: numerical simulations, radiative forcing estimates, and size-resolved parameterization scheme. *Atmos. Chem. Phys.* **21**, 12989–13010 (2021).

37. Mackowski, D. W. & Mishchenko, M. I. A multiple sphere T-matrix Fortran code for use on parallel computer clusters. *J. Quant. Spectrosc. Radiat. Transf.* **112**, 2182–2192 (2011).

38. Wang, Y. et al. Constructing shapes and mixing structures of black carbon particles with applications to optical calculations. *J. Geophys. Res.* **126**, e2021JD034620 (2021).

39. Hu, K. et al. Measurements of the diversity of shape and mixing state for ambient black carbon particles. *Geophys. Res. Lett.* **48**, e2021GL094522 (2021).

40. Slowik, J. G. et al. Measurements of morphology changes of fractal soot particles using coating and denuding experiments: implications for optical absorption and atmospheric lifetime. *Aerosp. Sci. Technol.* **41**, 734–750 (2007).

41. Schnitzler, E. G., Dutt, A., Charbonneau, A. M., Olfert, J. S. & Jäger, W. Soot aggregate restructuring due to coatings of secondary organic aerosol derived from aromatic precursors. *Environ. Sci. Technol.* **48**, 14309–14316 (2014).

42. Sedlacek, A. J. III, Lewis, E. R., Kleinman, L., Xu, J. & Zhang, Q. Determination of and evidence for non-core-shell structure of particles containing black carbon using the single-particle soot photometer (SP2). *Geophys. Res. Lett*. **39**, L06802 (2012).

43. Zhang, Y. et al. Extremely low-volatility organic coating leads to underestimation of black carbon climate impact. *One Earth* **6**, 158–166 (2023).

44. Naseri, A., Sipkens, T. A., Rogak, S. N. & Olfert, J. S. An improved inversion method for determining two-dimensional mass distributions of non-refractory materials on refractory black carbon. *Aerosp. Sci. Technol.* **55**, 104–118 (2020).

45. Liu, D. et al. Black-carbon absorption enhancement in the atmosphere determined by particle mixing state. *Nat. Geosci.* **10**, 184–188 (2017).

46. Zhai, J. et al. Absorption enhancement of black carbon aerosols constrained by mixing-state heterogeneity. *Environ. Sci. Technol.* **56**, 1586–1593 (2022).

47. Schwarz, J. P. et al. Coatings and their enhancement of black carbon light absorption in the tropical atmosphere. *J. Geophys. Res*. **113** https://doi.org/10.1029/2007jd009042 (2008).

48. Pratt, K. A. & Prather, K. A. Mass spectrometry of atmospheric aerosols—recent developments and applications. Part II: on-line mass spectrometry techniques. *Mass Spectrom. Rev.* **31**, 17–48 (2012).

49. Zelenyuk, A. & Imre, D. Beyond single particle mass spectrometry: multidimensional characterisation of individual aerosol particles. *Annu. Rev. Phys. Chem.* **28**, 309–358 (2009).

50. Canagaratna, M. R. et al. Chemical and microphysical characterization of ambient aerosols with the aerodyne aerosol mass spectrometer. *Mass Spectrom. Rev.* **26**, 185–222 (2007).

51. Virtanen, A. et al. An amorphous solid state of biogenic secondary organic aerosol particles. *Nature* **467**, 824–827 (2010).

52. China, S., Mazzoleni, C., Gorkowski, K., Aiken, A. C. & Dubey, M. K. Morphology and mixing state of individual freshly emitted wildfire carbonaceous particles. *Nat. Commun.* **4**, 2122 (2013).

53. Shi, Z. B., Zhang, D. Z., Ji, H. Z., Hasegawa, S. & Hayashi, M. Modification of soot by volatile species in an urban atmosphere. *Sci. Total Environ.* **389**, 195–201 (2008).

54. Geng, H., Ryu, J. Y., Maskey, S., Jung, H. J. & Ro, C. U. Characterisation of individual aerosol particles collected during a haze episode in Incheon, Korea using the quantitative ED-EPMA technique. *Atmos. Chem. Phys.* **11**, 1327–1337 (2011).

55. Ebert, M., Weinbruch, S., Hoffmann, P. & Ortner, H. M. The chemical composition and complex refractive index of rural and urban influenced aerosols determined by individual particle analysis. *Atmos. Environ.* **38**, 6531–6545 (2004).

56. Wang, Y. et al. Fractal dimensions and mixing structures of soot particles during atmospheric processing. *Environ. Sci. Tech. Let.* **4**, 487–493 (2017).

57. Ueda, S. et al. Morphological features and mixing states of soot-containing particles in the marine boundary layer over the Indian and Southern oceans. *Atmos. Chem. Phys.* **18**, 9207–9224 (2018).

58. Li, W. et al. A conceptual framework for mixing structures in individual aerosol particles. *J. Geophys. Res.* **121**, 13,784–713,798 (2016).

59. Pöhlker, C. et al. Biogenic potassium salt particles as seeds for secondary organic aerosol in the Amazon. *Science* **337**, 1075–1078 (2012).

60. Li, W. et al. Microscopic evidence for phase separation of organic species and inorganic salts in fine ambient aerosol particles. *Environ. Sci. Technol.* **55**, 2234–2242 (2021).

61. O'Brien, R. E. et al. Liquid–liquid phase separation in aerosol particles: imaging at the nanometer scale. *Environ. Sci. Technol.* **49**, 4995–5002 (2015).

62. Laskina, O., Young, M. A., Kleiber, P. D. & Grassian, V. H. Infrared extinction spectroscopy and micro-Raman spectroscopy of select components of mineral dust mixed with organic compounds. *J. Geophys. Res.* **118**, 6593–6606 (2013).

63. Takahama, S., Liu, S. & Russell, L. M. Coatings and clusters of carboxylic acids in carbon-containing atmospheric particles from spectromicroscopy and their implications for cloud-nucleating and optical properties. *J. Geophys. Res*. **115** https://doi.org/10.1029/2009jd012622 (2010).

64. Wang, M., Zheng, N., Zhao, D., Shang, J. & Zhu, T. Using micro-Raman spectroscopy to investigate chemical composition, mixing states, and heterogeneous reactions of individual atmospheric particles. *Environ. Sci. Technol.* **55**, 10243–10254 (2021).

65. Li, X., Gupta, D., Lee, J., Park, G. & Ro, C.-U. Real-time investigation of chemical compositions and hygroscopic properties of aerosols generated from NaCl and malonic acid mixture solutions using in situ Raman microspectrometry. *Environ. Sci. Technol.* **51**, 263–270 (2017).

66. Li, W. et al. Organic coating reduces hygroscopic growth of phase-separated aerosol particles. *Environ. Sci. Technol.* **55**, 16339–16346 (2021).

67. Ott, E. J. E., Tackman, E. C. & Freedman, M. A. Effects of sucrose on phase transitions of organic/inorganic aerosols. *ACS Earth Space Chem.* **4**, 591–601 (2020).

68. Kucinski, T. M., Dawson, J. N. & Freedman, M. A. Size-dependent liquid–liquid phase separation in atmospherically relevant complex systems. *J. Phys. Chem. Lett.* **10**, 6915–6920 (2019).

69. Zhang, J. et al. Liquid-liquid phase separation reduces radiative absorption by aged black carbon aerosols. *Commun. Earth Environ.* **3**, 128 (2022).

70. Veghte, D. P., Altaf, M. B. & Freedman, M. A. Size dependence of the structure of organic aerosol. *J. Am. Chem. Soc.* **135**, 16046–16049 (2013).

71. Pang, Y. et al. Quantifying the fractal dimension and morphology of individual atmospheric soot aggregates. *J. Geophys. Res.* **127**, e2021JD036055 (2022).

72. Chakrabarty, R. K., Moosmüller, H., Arnott, W. P., Garro, M. A. & Walker, J. Structural and fractal properties of particles emitted from spark ignition engines. *Environ. Sci. Technol.* **40**, 6647–6654 (2006).

73. Brasil, A. M., Farias, T. L. & Carvalho, M. G. A recipe for image characterization of fractal-like aggregates. *J. Aerosol Sci.* **30**, 1379–1389 (1999).

74. Adachi, K., Chung, S. H., Friedrich, H. & Buseck, P. R. Fractal parameters of individual soot particles determined using electron tomography: implications for optical properties. *J. Geophys. Res.* **112**, D14202 (2007).

75. Sipkens, T. A. et al. Overview of methods to characterize the mass, size, and morphology of soot. *J. Aerosol Sci.* **173**, 106211 (2023).

76. Haffner-Staton, E., Avanzini, L., La Rocca, A., Pfau, S. A. & Cairns, A. Automated particle recognition for engine soot nanoparticles. *J. Microsc.* **288**, 28–39 (2022).

77. Pang, Y. et al. Morphology and fractal dimension of size-resolved soot particles emitted from combustion sources. *J. Geophys. Res.* **128**, e2022JD037711 (2023).

78. Niu, H., Shao, L. & Zhang, D. Soot particles at an elevated site in eastern China during the passage of a strong cyclone. *Sci. Total Environ.* **430**, 217–222 (2012).

79. China, S., Salvadori, N. & Mazzoleni, C. Effect of traffic and driving characteristics on morphology of atmospheric soot particles at freeway on-ramps. *Environ. Sci. Technol.* **48**, 3128–3135 (2014).

80. Chen, C. et al. An unexpected restructuring of combustion soot aggregates by subnanometer coatings of polycyclic aromatic hydrocarbons. *Geophys. Res. Lett.* **43**, 11,080–011,088 (2016).

81. Zhang, J. et al. Structural collapse and coating composition changes of soot particles during long-range transport. *J. Geophys. Res.* **128**, e2023JD038871 (2023).

82. Enekwizu, O. Y., Hasani, A. & Khalizov, A. F. Vapor condensation and coating evaporation are both responsible for soot aggregate restructuring. *Environ. Sci. Technol.* **55**, 8622–8630 (2021).

83. Corbin, J. C., Modini, R. L. & Gysel-Beer, M. Mechanisms of soot-aggregate restructuring and compaction. *Aerosol Sci. Technol.* **57**, 89–111 (2023).

84. Zhang, R. Y. et al. Variability in morphology, hygroscopicity, and optical properties of soot aerosols during atmospheric processing. *Proc. Natl Acad. Sci. USA* **105**, 10291–10296 (2008).

85. Ma, X., Zangmeister, C. D., Gigault, J., Mulholland, G. W. & Zachariah, M. R. Soot aggregate restructuring during water processing. *J. Aerosol Sci.* **66**, 209–219 (2013).

86. Bhandari, J. et al. Extensive soot compaction by cloud processing from laboratory and field observations. *Sci. Rep.* **9**, 11824 (2019).

87. Chen, X. et al. Quantifying evolution of soot mixing state from transboundary transport of biomass burning emissions. *iScience* **26**, 108125 (2023).

88. Wu, Z. et al. Aerosol liquid water driven by anthropogenic inorganic salts: implying its key role in haze formation over the North China Plain. *Environ. Sci. Technol. Lett.* **5**, 160–166 (2018).

89. Peckhaus, A., Grass, S., Treuel, L. & Zellner, R. Deliquescence and efflorescence behavior of ternary inorganic/Organic/water aerosol particles. *J. Phys. Chem. A* **116**, 6199–6210 (2012).

90. Freney, E. J., Adachi, K. & Buseck, P. R. Internally mixed atmospheric aerosol particles: hygroscopic growth and light scattering. *J. Geophys. Res.* **115** https://doi.org/10.1029/2009jd013558 (2010).

91. Kuang, Y. et al. Deliquescent phenomena of ambient aerosols on the North China Plain. *Geophys. Res. Lett.* **43**, 8744–8750 (2016).

92. Posfai, M. et al. Atmospheric tar balls: particles from biomass and biofuel burning. *J. Geophys. Res.* **109** https://doi.org/10.1029/2003JD004169 (2004).

93. Wang, B. et al. Airborne soil organic particles generated by precipitation. *Nat. Geosci.* **9**, 433–437 (2016).

94. Sedlacek Iii, A. J. et al. Formation and evolution of tar balls from northwestern US wildfires. *Atmos. Chem. Phys.* **18**, 11289–11301 (2018).

95. Adachi, K. et al. Spherical tarball particles form through rapid chemical and physical changes of organic matter in biomass-burning smoke. *Proc. Natl Acad. Sci. USA* **116**, 19336–19341 (2019).

96. Liu, L. et al. Persistent residential burning-related primary organic particles during wintertime hazes in North China: insights into their aging and optical changes. *Atmos. Chem. Phys.* **21**, 2251–2265 (2021).

97. Li, C. et al. Dynamic changes in optical and chemical properties of tar ball aerosols by atmospheric photochemical aging. *Atmos. Chem. Phys.* **19**, 139–163 (2019).

98. Corbin, J. C. & Gysel-Beer, M. Detection of tar brown carbon with a single particle soot photometer (SP2). *Atmos. Chem. Phys.* **19**, 15673–15690 (2019).

99. You, Y. et al. Images reveal that atmospheric particles can undergo liquid–liquid phase separations. *Proc. Natl Acad. Sci. USA* **109**, 13188–13193 (2012).

100. Kirpes, R. M. et al. Solid organic-coated ammonium sulfate particles at high relative humidity in the summertime Arctic atmosphere. *Proc. Natl Acad. Sci. USA* **119**, e2104496119 (2022).

101. Shiraiwa, M. et al. Size distribution dynamics reveal particle-phase chemistry in organic aerosol formation. *Proc. Natl Acad. Sci. USA* **110**, 11746–11750 (2013).

102. Pajunoja, A. et al. Phase state of ambient aerosol linked with water uptake and chemical aging in the southeastern US. *Atmos. Chem. Phys.* **16**, 11163–11176 (2016).

103. Fu, Y. et al. Impact of cloud process in the mixing state and microphysical properties of soot particles: implications in light absorption enhancement. *J. Geophys. Res.* **127**, e2022JD037169 (2022).

104. Wu, Y. et al. Light absorption enhancement of black carbon aerosol constrained by particle morphology. *Environ. Sci. Technol.* **52**, 6912–6919 (2018).

105. Yuan, Q. et al. Evidence for large amounts of brown carbonaceous tarballs in the Himalayan atmosphere. *Environ. Sci. Technol. Lett.* **8**, 16–23 (2021).

106. Hoffer, A., Tóth, A., Nyirő-Kósa, I., Pósfai, M. & Gelencsér, A. Light absorption properties of laboratory-generated tar ball particles. *Atmos. Chem. Phys.* **16**, 239–246 (2016).

107. Jimenez, J. L. et al. Evolution of organic aerosols in the atmosphere. *Science* **326**, 1525–1529 (2009).

108. Fierce, L., Bond, T. C., Bauer, S. E., Mena, F. & Riemer, N. Black carbon absorption at the global scale is affected by particle-scale diversity in composition. *Nat. Commun.* **7**, 12361 (2016).

109. Peng, J. et al. Markedly enhanced absorption and direct radiative forcing of black carbon under polluted urban environments. *Proc. Natl Acad. Sci. USA* **113**, 4266–4267 (2016).

110. Farias, T. L., Köylü, Ü. Ö. & Carvalho, M. G. Range of validity of the Rayleigh–Debye–Gans theory for optics of fractal aggregates. *Appl. Opt.* **35**, 6560–6567, (1996).

111. Kelesidis, G. A., Neubauer, D., Fan, L. S., Lohmann, U. & Pratsinis, S. E. Enhanced light absorption and radiative forcing by black carbon agglomerates. *Environ. Sci. Technol.* **56**, 8610–8618 (2022).

112. Draine, B. T. & Flatau, P. J. Discrete-dipole approximation for scattering calculations. *J. Opt. Soc. Am. A* **11**, 1491–1499, (1994).

113. Liu, C., Chung, C. E., Yin, Y. & Schnaiter, M. The absorption Ångström exponent of black carbon: from numerical aspects. *Atmos. Chem. Phys.* **18**, 6259–6273 (2018).

114. Zaveri, R. A., Easter, R. C., Fast, J. D. & Peters, L. K. Model for simulating aerosol interactions and chemistry (MOSAIC). *J. Geophys. Res*. **113** https://doi.org/10.1029/2007JD008782 (2008).

115. Curtis, J. H., Riemer, N. & West, M. A single-column particle-resolved model for simulating the vertical distribution of aerosol mixing state: WRF-PartMC-MOSAIC-SCM v1.0. *Geosci. Model Dev.* **10**, 4057–4079 (2017).

116. Liu, X. et al. Toward a minimal representation of aerosols in climate models: description and evaluation in the Community Atmosphere Model CAM5. *Geosci. Model Dev.* **5**, 709–739 (2012).

117. Liu, X. et al. Description and evaluation of a new four-mode version of the Modal Aerosol Module (MAM4) within version 5.3 of the Community Atmosphere Model. *Geosci. Model Dev.* **9**, 505–522 (2016).

118. Collow, A. B. et al. Benchmarking GOCART-2G in the Goddard Earth Observing System (GEOS). *Geosci. Model Dev. Discuss.* **2023**, 1–47 (2023).

119. Matsui, H., Koike, M., Kondo, Y., Fast, J. D. & Takigawa, M. Development of an aerosol microphysical module: aerosol two-dimensional bin module for formation and aging simulation (ATRAS). *Atmos. Chem. Phys.* **14**, 10315–10331 (2014).

120. Kaiser, J. C. et al. The MESSy aerosol submodel MADE3 (v2.0b): description and a box model test. *Geosci. Model Dev.* **7**, 1137–1157 (2014).

121. Grandey, B. S. et al. Effective radiative forcing in the aerosol–climate model CAM5.3-MARC-ARG. *Atmos. Chem. Phys.* **18**, 15783–15810 (2018).

122. Chen, G. et al. An aerosol optical module with observation-constrained black carbon properties for global climate models. *J. Adv. Model Earth Syst*. **15** https://doi.org/10.1029/2022ms003501 (2023).

123. Andersson, E. & Kahnert, M. Coupling aerosol optics to the MATCH (v5.5.0) chemical transport model and the SALSA (v1) aerosol microphysics module. *Geosci. Model Dev.* **9**, 1803–1826 (2016).

124. Kahnert, M. & Kanngießer, F. Modelling optical properties of atmospheric black carbon aerosols. *J. Quant. Spectrosc. Radiat. Transf.* **244**, 106849 (2020).

125. Chakrabarty, R. K. & Heinson, W. R. Scaling laws for light absorption enhancement due to nonrefractory coating of atmospheric black carbon aerosol. *Phys. Rev. Lett.* **121**, 218701 (2018).

126. Zhang, X., Mao, M., Yin, Y. & Tang, S. The absorption Ångstrom exponent of black carbon with brown coatings: effects of aerosol microphysics and parameterization. *Atmos. Chem. Phys.* **20**, 9701–9711 (2020).

127. Cappa, C. D. et al. Light absorption by ambient black and brown carbon and its dependence on black carbon coating state for two California, USA, cities in winter and summer. *J. Geophys. Res.* **124**, 1550–1577 (2019).

128. Liu, S. et al. Enhanced light absorption by mixed source black and brown carbon particles in UK winter. *Nat. Commun.* **6**, 8435 (2015).

129. Radney, J. G. et al. Dependence of soot optical properties on particle morphology: measurements and model comparisons. *Environ. Sci. Technol.* **48**, 3169–3176 (2014).

130. Moffet, R. C. & Prather, K. A. In-situ measurements of the mixing state and optical properties of soot with implications for radiative forcing estimates. *Proc. Natl Acad. Sci. USA* **106**, 11872–11877 (2009).

131. Schnaiter, M. et al. Absorption amplification of black carbon internally mixed with secondary organic aerosol. *J. Geophys. Res.* **110**, D19204 (2005).

132. Luo, J. et al. Optical modeling of black carbon with different coating materials: the effect of coating configurations. *J. Geophys. Res.* **124**, 13230–13253 (2019).

133. Zeng, L. et al. Overestimation of black carbon light absorption due to mixing state heterogeneity. *npj Clim. Atmos. Sci*. **7** https://doi.org/10.1038/s41612-023-00535-8 (2024).

134. Fard, M. M., Krieger, U. K. & Peter, T. Shortwave radiative impact of liquid–liquid phase separation in brown carbon aerosols. *Atmos. Chem. Phys.* **18**, 13511–13530 (2018).

135. Huang, X. F. et al. Microphysical complexity of black carbon particles restricts their warming potential. *One Earth* https://doi.org/10.1016/j.oneear.2023.12.004 (2023).

136. Lohmann, U. et al. Future warming exacerbated by aged-soot effect on cloud formation. *Nat. Geosci.* **13**, 674–680 (2020).

137. Christensen, M. W. et al. Opportunistic experiments to constrain aerosol effective radiative forcing. *Atmos. Chem. Phys.* **22**, 641–674 (2022).

138. Myhre, G. et al. Radiative forcing of the direct aerosol effect from AeroCom Phase II simulations. *Atmos. Chem. Phys.* **13**, 1853–1877 (2013).

139. Thornhill, G. D. et al. Effective radiative forcing from emissions of reactive gases and aerosols—a multi-model comparison. *Atmos. Chem. Phys.* **21**, 853–874 (2021).

140. Wang, X. et al. Exploiting simultaneous observational constraints on mass and absorption to estimate the global direct radiative forcing of black carbon and brown carbon. *Atmos. Chem. Phys.* **14**, 10989–11010 (2014).

141. Samset, B. H. et al. Modelled black carbon radiative forcing and atmospheric lifetime in AeroCom Phase II constrained by aircraft observations. *Atmos. Chem. Phys.* **14**, 12465–12477 (2014).

142. Kipling, Z. et al. Constraints on aerosol processes in climate models from vertically-resolved aircraft observations of black carbon. *Atmos. Chem. Phys.* **13**, 5969–5986 (2013).

143. Matsui, H., Hamilton, D. S. & Mahowald, N. M. Black carbon radiative effects highly sensitive to emitted particle size when resolving mixing-state diversity. *Nat. Commun.* **9**, 3446 (2018).

144. Ramanathan, V. & Carmichael, G. Global and regional climate changes due to black carbon. *Nat. Geosci.* **1**, 221–227 (2008).

145. Feng, Y., Ramanathan, V. & Kotamarthi, V. R. Brown carbon: a significant atmospheric absorber of solar radiation? *Atmos. Chem. Phys.* **13**, 8607–8621 (2013).

146. Wang, R. et al. Estimation of global black carbon direct radiative forcing and its uncertainty constrained by observations. *J. Geophys. Res.* **121**, 5948–5971 (2016).

147. Saleh, R. et al. Contribution of brown carbon and lensing to the direct radiative effect of carbonaceous aerosols from biomass and biofuel burning emissions. *J. Geophys. Res.* **120**, 2015JD023697 (2015).

148. Lin, G., Sillman, S., Penner, J. E. & Ito, A. Global modeling of SOA: the use of different mechanisms for aqueous-phase formation. *Atmos. Chem. Phys.* **14**, 5451–5475 (2014).

149. Hammer, M. S. et al. Interpreting the ultraviolet aerosol index observed with the OMI satellite instrument to understand absorption by organic aerosols: implications for atmospheric oxidation and direct radiative effects. *Atmos. Chem. Phys.* **16**, 2507–2523 (2016).

150. Drugé, T. et al. Modeling radiative and climatic effects of brown carbon aerosols with the ARPEGE-Climat global climate model. *Atmos. Chem. Phys.* **22**, 12167–12205 (2022).

151. Bellouin, N. et al. Bounding global aerosol radiative forcing of climate change. *Rev. Geophys.* **58**, e2019RG000660 (2020).

152. Schill, G. P. et al. The contribution of black carbon to global ice nucleating particle concentrations relevant to mixed-phase clouds. *Proc. Natl. Acad. Sci. USA* **117**, 202001674 (2020).

153. Jesús et al. Is black carbon an unimportant ice-nucleating particle in mixed-phase clouds? *J. Geophys. Res.* **123**, 4273–4283 (2018).

154. Levin, E. J. T. et al. Ice-nucleating particle emissions from biomass combustion and the potential importance of soot aerosol. *J. Geophys. Res.* **121**, 5888–5903 (2016).

155. Friedman, B. et al. Ice nucleation and droplet formation by bare and coated soot particles. *J. Geophys. Res.* **116**, D17203 (2011).

156. Kupiszewski, P. et al. Ice residual properties in mixed-phase clouds at the high-alpine Jungfraujoch site. *J. Geophys. Res.* **121**, 12,343–312,362 (2016).

157. Kulkarni, G. et al. Ice nucleation activity of diesel soot particles at cirrus relevant temperature conditions: effects of hydration, secondary organics coating, soot morphology, and coagulation. *Geophys. Res. Lett.* **43**, 3580–3588 (2016).

158. Cozic, J. et al. Black carbon enrichment in atmospheric ice particle residuals observed in lower tropospheric mixed phase clouds. *J. Geophys. Res.* **113**, D15209 (2008).

159. Twohy, C. H., Anderson, J. R. & Crozier, P. A. Nitrogenated organic aerosols as cloud condensation nuclei. *Geophy. Res. Lett*. **32** https://doi.org/10.1029/2005GL023605 (2005).

160. Koch, D. et al. Soot microphysical effects on liquid clouds, a multi-model investigation. *Atmos. Chem. Phys.* **11**, 1051–1064 (2011).

161. McNeill, V. F., Sareen, N. & Schwier, A. *Topics in Current Chemistry* Ch. 404, 1–59 (Springer, 2013).

162. Wang, J. et al. Cloud droplet activation of secondary organic aerosol is mainly controlled by molecular weight, not water solubility. *Atmos. Chem. Phys.* **19**, 941–954 (2019).

163. Wokosin, K. A., Schell, E. L. & Faust, J. A. Surfactants, films, and coatings on atmospheric aerosol particles: a review. *Environ. Sci. Atmos*. https://doi.org/10.1039/D2EA00003B (2022).

164. Knopf, D. A. et al. Microspectroscopic imaging and characterization of individually identified ice nucleating particles from a case field study. *J. Geophys. Res.* **119**, 2014JD021866 (2014).

165. Dong, Z. et al. Variability in individual particle structure and mixing states between the glacier–snowpack and atmosphere in the northeastern Tibetan Plateau. *Cryosphere* **12**, 3877–3890 (2018).

166. He, C. et al. Impact of grain shape and multiple black carbon internal mixing on snow albedo: parameterization and radiative effect analysis. *J. Geophys. Res.* **123**, 1253–1268 (2018).

167. Johansson, K. O., Head-Gordon, M. P., Schrader, P. E., Wilson, K. R. & Michelsen, H. A. Resonance-stabilized hydrocarbon-radical chain reactions may explain soot inception and growth. *Science* **361**, 997–1000 (2018).

168. Ching, J., Kajino, M. & Matsui, H. Resolving aerosol mixing state increases accuracy of black carbon respiratory deposition estimates. *One Earth* **3**, 763–776 (2020).

169. Zheng, Z. et al. Estimating submicron aerosol mixing state at the global scale with machine learning and earth system modeling. *Earth Space Sci*. **8** https://doi.org/10.1029/2020ea001500 (2021).

170. Luo, J., Zhang, Y., Wang, F., Wang, J. & Zhang, Q. Applying machine learning to estimate the optical properties of black carbon fractal aggregates. *J. Quant. Spectrosc. Radiat. Transf.* **215**, 1–8 (2018).

171. Lamb, K. D. & Gentine, P. Zero-shot learning of aerosol optical properties with graph neural networks. *Sci. Rep.* **13**, 18777 (2023).

172. Wang, X., Bi, L., Han, W. & Zhang, X. Single-scattering properties of encapsulated fractal black carbon particles computed using the invariant imbedding T-matrix method and deep learning approaches. *J. Geophys. Res.* **128**, e2023JD039568 (2023).

173. Shen, W. et al. Improving BC mixing state and CCN activity representation with machine learning in the Community Atmosphere Model Version 6 (CAM6). *J. Adv. Model Earth Syst*. **16** https://doi.org/10.1029/2023ms003889 (2024).

174. Gorkowski, K., Donahue, N. M. & Sullivan, R. C. Aerosol optical tweezers constrain the morphology evolution of liquid-liquid phase-separated atmospheric particles. *Chem* **6**, 204–220 (2020).

175. Dazzi, A. & Prater, C. B. AFM-IR: technology and applications in nanoscale infrared spectroscopy and chemical imaging. *Chem. Rev.* **117**, 5146–5173 (2017).

176. Yuan, Q. et al. Mixing state and fractal dimension of soot particles at a remote site in the Southeastern Tibetan plateau. *Environ. Sci. Technol.* **53**, 8227–8234 (2019).

177. Raatikainen, T. et al. Size-selected black carbon mass distributions and mixing state in polluted and clean environments of northern India. *Atmos. Chem. Phys.* **17**, 371–383 (2017).

178. Fraund, M. et al. Elemental mixing state of aerosol particles collected in Central Amazonia during GoAmazon2014/15. *Atmosphere* **8**, 173 (2017).

179. Ljungman, P. L. S. et al. Long-term exposure to particulate air pollution, black carbon, and their source components in relation to ischemic heart disease and stroke. *Environ. Health Perspect.* **127**, 107012 (2019).

180. Zhu, S., Zhang, H., Zhou, C., Wei, X. & Liu, Y. Optical properties of mixed black and brown carbon aerosols. *Opt. Express* **30**, 33588–33602 (2022).

Author contributions
W.L. led the review. N.R., W.L., L.X., Y.W. and A.L. prepared Figs. 1–4 and contributed to the laboratory experiment parts. W.L. and A.L. wrote the draft and designed Fig. 5. A.L. and Z.S. contributed Fig. 6. Z.S., D.Z., Z.Z. and A.L. contributed to experimental parts, interpretation, and writing. K.A. and N.R. contributed to modeling parts, interpretation, and writing. All authors contributed to manuscript preparation, interpretation, discussion, and writing.

Competing interests
The authors declare no competing interests.

Additional information
Correspondence and requests for materials should be addressed to Weijun Li or Alexander Laskin.

Reprints and permissions information is available at http://www.nature.com/reprints

Publisher's note Springer Nature remains neutral with regard to jurisdictional claims in published maps and institutional affiliations.